JOURNAL OF AIRCRAFT
Vol. 44, No. 1, January–February 2007

Design of Waverider Configuration with High Lift-Drag Ratio

Wang Yankui,* Yang Shuifeng,† Zhang Dongjun,‡ and Deng Xueying§
Beijing University of Aeronautics and Astronautics, 100083 Beijing, People's Republic of China

DOI: 10.2514/1.22669

As an ideal configuration with a high lift-drag ratio, the waverider has become one kind of an attracted configuration for some special purposes. The main purpose of this paper is to investigate the design method for a cone-derived waverider at Ma = 6 and its basic aerodynamic characteristics, especially the improvement of the configuration for a higher lift-drag ratio. The investigation is finished by CFD and shows that first, the inverse-design method for the waverider configuration based on an inviscid conical shock wave is successful. Secondly, a great improvement of the lift-drag ratio from 2.95 to 4.06 can be obtained by modifying the prototype configuration.

Nomenclature

C_D = drag coefficient, $D/(qS_{\text{ref}})$
C_L = lift coefficient, $L/(qS_{\text{ref}})$
K = lift-drag ratio, C_L/C_D
Ma = freestream Mach number
q = dynamic pressure
S_{ref} = reference area
α = attack angle, deg
ρ = atmosphere density
v = freestream velocity

I. Introduction

WITH the demand for reliable, cost effective launch services steadily increasing, the conceptual design of next generation launch vehicles is underway. The single-stage-to-orbit (SSTO) vehicle is thereby becoming very important. High lift-drag ratio is necessary and important to all of the supersonic or hypersonic vehicle concepts currently under investigation, especially for the SSTO vehicle [1–6]. A waverider is a kind of advanced lifting body that possesses the highest lift-drag ratio of all known hypersonic vehicles and is well suited for sustained cruise applications. When operating at on-design conditions, in the supersonic or hypersonic regime, these configurations have an attached shock wave along their leading edge allowing the high pressure flowfield to be contained beneath the vehicle and avoiding "leakage" of high pressure gas to the lower pressure flowfield so that a high lift-drag ratio is expected to be provided. The waverider has become an ideal candidate for interplanetary space exploration with applications to reusable launch vehicles, transatmospheric space planes, and defense missiles [7–16]. The main purpose of this paper is to study the design method for a cone-derived waverider prototype with a high lift-drag ratio at on-design conditions of Ma = 6 and its basic aerodynamic characteristics [17,18]. In addition, the modified configuration of a waverider by expanding the upper surface of the waverider prototype has been constructed and a great improvement of the lift-drag ratio from 2.95 to 4.06 can be obtained. As a result, a waverider configuration with high lift-drag ratio is developed as a primary basis for the design of a hypersonic vehicle with rocket propulsion, and this is the main purpose for some special utility.

Presented as Paper 6040 at the AIAA Atmospheric Flight Mechanics Conference and Exhibit, Hyatt Regency San Francisco at Embarcadero Center, San Francisco, California, ; received 24 January 2006; revision received 4 May 2006; accepted for publication 5 May 2006.

*Professor, Institute of Fluid Mechanics, 37#, xueyuanlu, Haidian District.
†Graduate Student.
‡Graduate Student.
§Professor, Senior Member AIAA.

II. Computational Method and Mesh

A. Computational Method

To investigate the aerodynamic performances of the developed waverider configuration, a CFD method is employed, which is based on a finite volume formulation of the Navier–Stokes equations. On these conditions of supersonic and hypersonic flows involving heat transfer and compressibility, an additional equation for energy conservation is solved. The equation for conservation of mass can be written as follows:

$$\frac{\partial \rho}{\partial t} + \nabla \cdot (\rho \boldsymbol{v}) = S_m \tag{1}$$

Equation (1) is the general form of the mass conservation equation and is valid for incompressible as well as compressible flows. The source S_m is the mass added to the continuous phase from the dispersed second phase.

The momentum conservation in an inertial reference frame is described by Eq. (2):

$$\frac{\partial}{\partial t}(\rho \boldsymbol{v}) + \nabla \cdot (\rho \boldsymbol{v}\boldsymbol{v}) = -\nabla p + \nabla \cdot (\boldsymbol{\tau}) + \rho \boldsymbol{g} + \boldsymbol{F} \tag{2}$$

where p is the static pressure, $\boldsymbol{\tau}$ is the stress tensor shown in Eq. (3), and $\rho \boldsymbol{g}$ and $\boldsymbol{F}$ are the gravitational body force and external body forces (e.g., that arise from interaction with the dispersed phase), respectively.

The stress tensor $\boldsymbol{\tau}$ is given as follows:

$$\tau = [\mu(\nabla \boldsymbol{v} + \nabla \boldsymbol{v}^T) - \tfrac{2}{3}\nabla \cdot \boldsymbol{v} I] \tag{3}$$

where μ is the molecular viscosity, I is the unit tensor, and the second term on the right-hand side is the effect of volume dilation.

The energy equation is as follows:

$$\frac{\partial}{\partial t}(\rho E) + \nabla \cdot [\boldsymbol{v}(\rho E + p)] = \nabla \cdot \left[k_{\text{eff}} \nabla T - \sum_j h_j \boldsymbol{J}_j + (\boldsymbol{\tau}_{\text{eff}} \cdot \boldsymbol{v}) \right] \tag{4}$$

where k_{eff} is the effective conductivity ($k + k_t$, where k_t is the turbulent thermal conductivity, defined according to the turbulence model being used), and $\boldsymbol{J}_j$ is the diffusion flux of species j. The first three terms on the right-hand side of Eq. (4) represent energy transfer

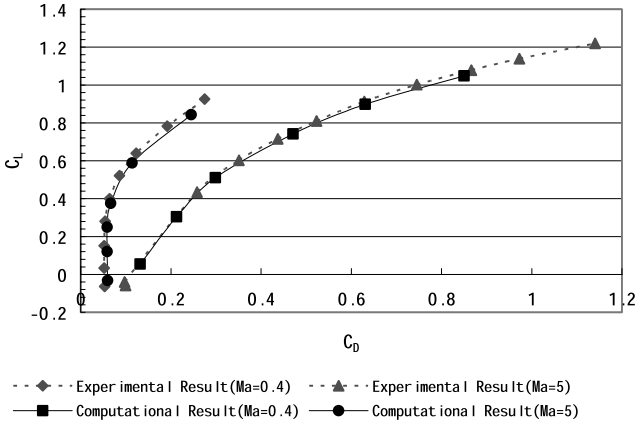

Fig. 1 Comparison of experimental results with computational results by the CFD method in this paper.

due to conduction, species diffusion, and viscous dissipation, respectively. And in Eq. (4)

$$E = h - \frac{p}{\rho} + \frac{v^2}{2} \tag{5}$$

where h is the sensible enthalpy for ideal gas.

The standard k–ε turbulent model is used in the computational investigation shown in Eq. (6):

$$\begin{cases} \rho \frac{Dk}{Dt} = \frac{\partial}{\partial x_i}[(\mu + \frac{\mu_t}{\sigma_k})\frac{\partial k}{\partial x_i}] + G_k + G_b - \rho\varepsilon - Y_M \\ \rho \frac{D\varepsilon}{dt} = \frac{\partial}{\partial x_i}[(\mu + \frac{\mu_t}{\sigma_\varepsilon})\frac{\partial \varepsilon}{\partial x_i}] + C_{1\varepsilon}\frac{\varepsilon}{k}(G_k + C_{3\varepsilon}G_b) - C_{2\varepsilon}\rho\frac{\varepsilon^2}{k} \end{cases} \tag{6}$$

where G_k is the generation of turbulence kinetic energy due to the mean velocity gradients. G_b is the generation of turbulence kinetic energy due to buoyancy. Y_M is the contribution of the fluctuating dilatation in compressible turbulence to the overall dissipation rate. $C_{1\varepsilon}$, $C_{2\varepsilon}$, and $C_{3\varepsilon}$ are constants. σ_k and σ_ε are the turbulent Prandtl numbers for k and ε, respectively.

B. Computational Mesh

Three-dimensional computational grids are developed for the waverider prototype and modified configuration. To reduce and neglect the influence of the magnitude of the uncertainty in the CFD calculation, multizone mesh volumes are adopted, and structured or unstructured grids are used in different computational regions. In addition, the computational meshes are kept the same except for the region very close to the upper surface, because very small differences between these two configurations, namely, waverider prototype and modified configuration, lie only on the upper surface of the model with or without a 3 deg expansion. The grid contains 180 points in the streamwise direction, 150 in the circumferential direction and 110 in the vertical direction. A no-slip boundary condition is applied to the walls with a fixed temperature of 300 K. In addition, the coupled and second-order upwind solver is used except that the freestream conditions are applied to the outer boundary and second-order extrapolation from the interior cells is applied to the exit plane.

The CFD method and program adopted in this paper is verified by an example of a kind of supersonic fighter configuration on conditions of $\mathrm{Ma} = 0.4$ and $\mathrm{Ma} = 5$ by comparison with the experimental results, shown in Fig. 1. The two group lines represent the variation of lift coefficient C_L with drag coefficient C_D on condition of $\mathrm{Ma} = 0.4$ and $\mathrm{Ma} = 5$, respectively; the solid lines stand for computational results and the dotted lines stand for experimental results. The conclusion can be drawn from Fig. 1 that the numerical estimates are shown to be in good agreement with the experimental results, and the CFD method used in these investigations is valid and reliable.

III. Design of the Waverider Prototype

A. Design Method

By definition, a waverider is a kind of supersonic lifting body that has a shock wave attached everywhere along its leading edges. In practice, a waverider configuration can always be designed from a known inviscid supersonic compression flowfield, such as a cone shock layer, and from that a stream surface starting from an arbitrary line on the shock wave can be formed. Finally the viscous effects and blunt leading edges resisting heat will be taken into account so that the developed configuration can be expected to meet the requirements of a supersonic or hypersonic cruise.

In this paper, the waverider prototype based on the cone-derived inviscid supersonic flowfield will be constructed by the inverse-design method on conditions of $\mathrm{Ma} = 6$ and $\alpha = 0$ deg first. Secondly, the upper surface of the waverider prototype will be modified by expanding it to improve its lift-drag ratio and the aerodynamic characteristics are given.

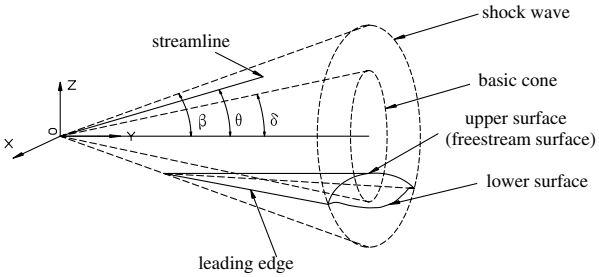

Fig. 2 The principle of the waverider design.

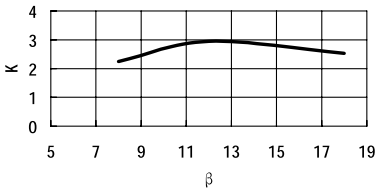

Fig. 3 The variation of lift-drag-ratio k with β.

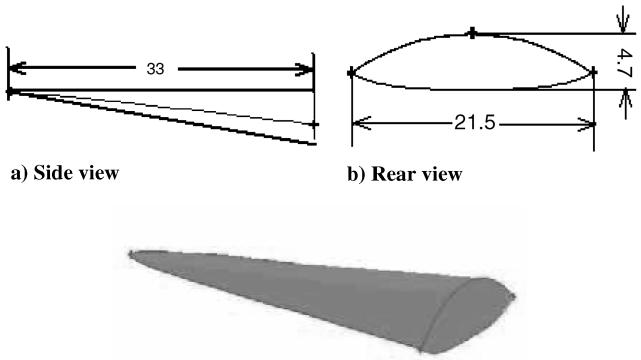

a) Side view **b) Rear view**

c) The three-dimensional configuration

Fig. 4 The sketch of the waverider prototype (dimensions in mm).

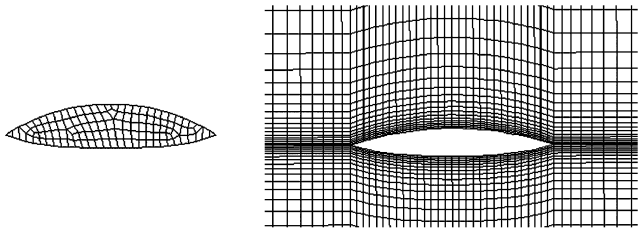

a) Rear view **b) Section plane in computed field**

Fig. 5 Computational grid.

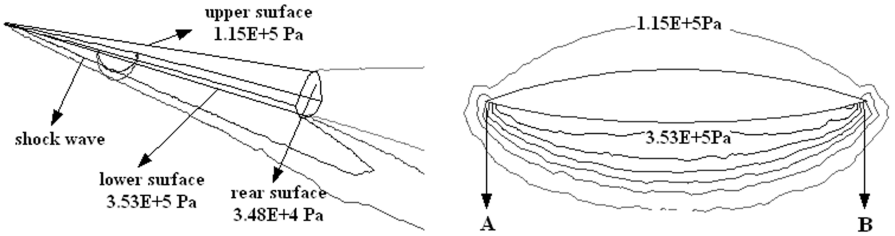

a) Surface and longitudinal symmetric plane b) One sectional plane

Fig. 6 Pressure isobar distribution of the waverider prototype (Ma = 6 and $\alpha = 0$ deg).

B. Design of the Waverider Prototype

In this paper, a cone-derived waverider prototype will be made. First, a basic inviscid supersonic cone shock is selected at Ma = 6 and zero angle of attack, as shown in Fig. 2, where δ is the half conical angle of the basic cone body, β is the basic conical shock wave angle, and θ is the streamline angle after the shock wave through a certain leading edge point. In practice, the basic conical shock wave angle β is the key parameter influencing the aerodynamic performances of the designed lifting body. Figure 3 gives the computational results of the lift-drag ratio (K) of the lifting body changing with β and shows that $\beta = 12$ deg is an ideal parameter for a waverider configuration with a high lift-drag ratio. The equation of the cone shock wave in the reference frame (shown in Fig. 2) when $\beta = 12$ deg is as follows:

$$x^2 + z^2 = 0.0451803y^2 \tag{7}$$

The next step in the lower surface design is to define a leading edge that lies on the conical shock wave. Thereby, a cylinder surface with $x^2 + (z + 30) = 20^2$ in the reference frame (shown in Fig. 2) is defined to intersect with the basic conical shock wave, and this cylinder surface must be keep entirely below the x–o–y plane of the basic shock wave to ensure that the resulting waverider configuration is a lifting body, shown in Fig. 2. The leading edge of the waverider in three-dimensional space is then defined as the intersection line of the cylinder upper surface with the basic conical shock wave. Third, once the leading edge has been defined, a series of points can be chosen along the leading edge from which the streamlines after the shock wave can be traced according to Eq. (8). And the lower surface of the waverider consists of these series of streamlines through the chosen points along the leading edge:

$$\begin{aligned}
&\frac{\partial^2 g}{\partial x^2} + \frac{\partial^2 g}{\partial z^2} - (\mathrm{Ma}^2 - 1)\frac{\partial^2 g}{\partial y^2} = 0\\
&\psi = \psi_n + \frac{2}{\gamma + 1}\frac{1}{M_a^2 \tan^2 \beta}\\
&\psi_n = \frac{\gamma - 1}{\gamma + 1} + \frac{2}{\gamma + 1}\frac{1}{M_a^2}\\
&\sin\theta = \left(1 - \frac{1}{2}\psi\right)\sin\beta\cos(\beta - \theta)
\end{aligned} \tag{8}$$

where g stands for flow speed, Ma is the freestream Mach number, ψ stands for density ratio before and after the shock wave, ψ_n stands for density ratio before and after the normal shock wave, θ is the streamline angle, and β is the basic conical shock wave angle.

Finally, the upper surface of the cylinder is defined as the upper surface of the waverider prototype in this paper. The final waverider prototype formed by the above inverse-design method is shown in Fig. 4.

C. Generation of the Computational Grid

By selecting an elliptical surface in the far field around the computed configuration, multizone mesh volumes are adopted with a different grid density for computational study of the aerodynamic performance of the above designed waverider prototype. The grid contains 180 points in the streamwise direction, 150 in the circumferential direction, and 110 in the vertical direction. To neglect the influence of the magnitude of the uncertainty in the CFD calculation, the computational meshes are kept the same except for the region very close to the upper surface. The difference between the waverider prototype and modified configuration lies only on the upper surface with or without a 3 deg expansion. The difference of the mesh distribution between these two configurations can be neglected by selecting the same point distribution on the leading edge, and structured grids are adopted near the configuration surface. The grid adopted in the computational investigation is shown in Fig. 5.

IV. Computational Results and Modified Configuration

A. Aerodynamic Characteristics of the Waverider Prototype

The main purpose of this paper is to investigate the aerodynamic performance of lift, drag, and lift-drag ratio of the waverider except for moments and side-force on-design conditions. The computational results of aerodynamic characteristics of the waverider prototype on the condition of Ma = 6 and $\alpha = 0$ deg are as follows: C_L has a value of 0.08860; C_D has a value of 0.03004; and K has a value of 2.95.

Figure 6 shows the pressure isobar distribution on the surface of the waverider prototype and one sectional plane in the flowfield. Several conclusions can be drawn from Fig. 6 such as the following:

1) There is a strong shock wave attached on the leading edge, therefore it is successful in designing this prototype configuration, shown in Fig. 6a.

2) Most of the region under the configuration has been filled with higher pressure ($3.53 \times 10^5 P_a$) than that on the upper surface ($1.15 \times 10^5 P_a$) of the waverider. Moreover this attached shock wave along its leading edge allows the high pressure flowfield to be contained beneath the lower surface and avoids leakage of high pressure gas to the lower pressure flowfield over the upper surface,

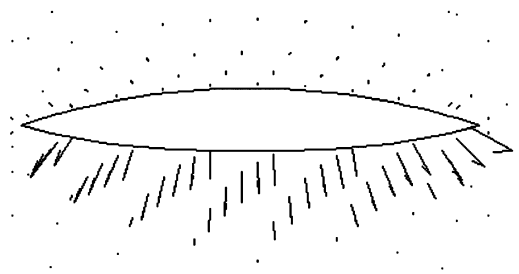

Fig. 7 Speed vector distribution on one section of the waverider prototype.

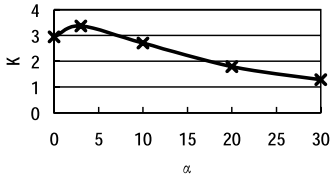

Fig. 8 The variation of lift-drag ratio k with α of the waverider prototype.

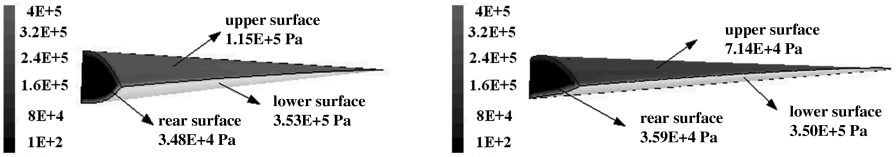

a) The pressure isobar of waverider prototype b) The pressure isobar of modified configuration

Fig. 9 The comparison of pressure distribution between the prototype and the modified configuration (Ma = 6 and $\alpha = 0$ deg).

which is illustrated in Fig. 6b. In addition, it can also be proved from the speed vector map of one section plane shown in Fig. 7.

3) The whole upper surface of the waverider, which is designed for a freestream surface, is full of the low pressure.

4) In the wake range behind the configuration, the pressure ($3.48 \times 10^4 P_a$) on the rear surface is lower than those on the upper and lower surfaces. Therefore a big inviscid drag (namely, pressure drag) is produced, which is about 0.02213 more than the viscous drag (0.00792) provided by viscous friction acting on all surfaces of the prototype configuration. But the viscous lift contribution of the whole model provided by the viscous friction is very small (−0.00069), far less than the inviscid lift contribution (0.08929) of the whole model provided by the pressure. Therefore, it is very important to reduce the inviscid drag contribution (pressure drag) in order to improve the lift-drag-ratio of the prototype configuration.

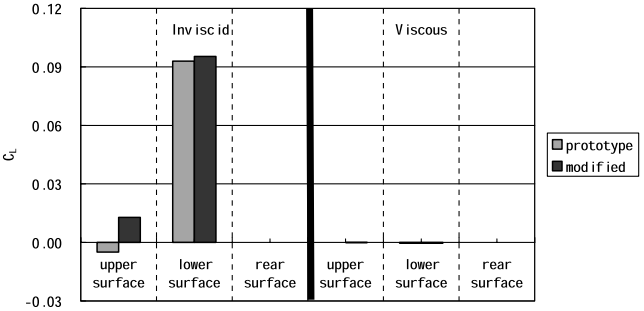

Fig. 10 Comparison of inviscid and viscous lift contribution of different parts between the prototype and the modified configuration (Ma = 6 and $\alpha = 0$ deg).

B. Aerodynamic Characteristics of the Modified Configuration

Figure 8 gives the curve of the lift-drag ratio (K) of the waverider prototype changing with the angle of attack. It can be found that the lift-drag ratio K begins increasing with the angle of attack and then decreasing. Therefore, there is a maximum lift-drag ratio $K_{\max}$ at about $\alpha = 3$ deg. In other words, a certain expansion on the upper surface is favorable for improving the performance of the waverider. Therefore the prototype configuration is modified with a 3 deg expansion angle on the upper surface of the prototype, named the modified configuration. On the design condition of Ma = 6 and $\alpha = 0$ deg, a larger lift-drag ratio $K_{\max} = 4.06$ is obtained and it is bigger than that of the prototype configuration. The computational results of the aerodynamic performances of the modified configuration are as follows: for C_L the value is 0.11059; for C_D the value is 0.02723; and for K the value is 4.06. The lift-drag ratio K and lift coefficient C_L have been improved by 37% and 25% more than that of the prototype configuration, respectively; moreover the drag coefficient C_D decreases by 10% less than that of the prototype configuration.

The pressure isobar distribution of the prototype and modified configuration of the waverider are shown in Fig. 9. First, the pressure on the upper surface of the modified configuration with a 3 deg expansion angle is about $7.14 \times 10^4 P_a$, which is less than that ($1.15 \times 10^5 P_a$) on the upper surface of the waverider prototype. But the pressure on the lower surface of these two kinds of waverider configurations is similar ($3.5 \times 10^5 P_a$). As a result, the inviscid lift contribution of the modified configuration provided by pressure is improved from 0.08929 to 0.11140, shown in Table 1. In addition, the inviscid drag contribution of the modified configuration provided by pressure is decreased from 0.02213 to 0.01994 due to the pressure increasing on the rear surface from $3.48 \times 10^4 P_a$ of the prototype configuration to $3.59 \times 10^4 P_a$ of the modified configuration by comparing Figs. 9a and 9b. Therefore the higher lift-drag ratio of the modified configuration has been obtained by expanding the upper surface of the waverider prototype.

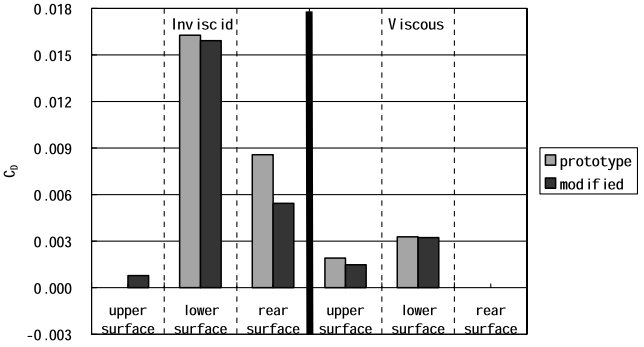

Fig. 11 Comparison of inviscid and viscous drag contribution of different parts between the prototype and the modified configuration (Ma = 6 and $\alpha = 0$ deg).

The distributions of the inviscid and viscous lift and drag contribution acting on different parts of the model and its comparison between the prototype and modified configuration at Ma = 6 and $\alpha = 0$ deg are shown in Figs. 10 and 11. As illustrated in Fig. 10, it is very clear that the lift increment of the modified configuration, compared with that of the prototype configuration, is mainly due to the static pressure decreasing caused by the expanded upper surface, and the expansion of the upper surface has no influence on the viscous lift contribution and little influence on the flowfield over the lower surface. On the other hand, the 10% drag reduction of the modified configuration, compared with that of the prototype configuration, is mainly caused by the inviscid drag contribution owing to the static pressure increasing acting on the rear surface of the modified configuration with little expense of the inviscid drag increment due to the adverse pressure gradient caused by the expansion of the upper surface. In addition, the inviscid drag

Table 1 The comparison of the lift and drag coefficients between the modified configuration and prototype at Ma = 6 and $\alpha = 0$ deg

Coefficient	C_L			C_D		
model	Pressure	Viscous	Total	Pressure	Viscous	Total
Prototype	0.08929	−0.00069	0.08860	0.02213	0.00791	0.03004
Modified configuration	0.11140	−0.00081	0.11059	0.01994	0.00730	0.02724

contribution due to the pressure distribution on the lower surface is evidently bigger than the viscous drag and accounts for more than 50% of the total drag for all the configurations. Therefore, a thorough investigation of how to reduce the inviscid drag acting on the lower surface of the waverider is needed to improve the aerodynamic performances of the waverider.

V. Conclusions

Several conclusions can be drawn from the above discussions:

1) The inverse-design method for the waverider configuration based on the inviscid conical shock wave is successful and the valuable results considering viscous effect can be obtained.

2) The biggest lift-drag ratio $K_{\max} = 2.95$ of the waverider prototype including viscous effects has been gotten at $\mathrm{Ma} = 6$ and zero angle of attack when the basic conical shock wave angle β is 12 deg.

3) A certain expansion on the upper surface of the prototype waverider is favorable for improving the lift-drag ratio K. And a great improvement of the lift-drag ratio from 2.95 to 4.06 can be obtained by modifying the prototype configuration with 3 deg expanding angle on the upper surface, This is mainly caused by the pressure decreasing on the upper surface and pressure increasing on the rear surface of the modified configuration.

4) The inviscid drag contribution due to the pressure distribution on the lower surface of the configuration is evidently bigger than viscous drag and accounts for more than 50% of the total drag for all the configurations. Therefore, a deep investigation of how to reduce the inviscid drag acting on the lower surface of the waverider is needed to get bigger improvement of the aerodynamic performances of the waverider.

References

[1] Blankson, M., "Air-Breathing Hypersonic Cruise Prospects for Mach 4-7 Waverider Aircraft," *Journal of Engineering for Gas Turbines and Power*, Vol. 116, No. 1, 1994, pp. 104–115.

[2] Miyagawa, T., Ohta, T., and Matsuzaki, R., "Experimental Studies on Several Waverider Configuration," *Journal of Aero Space Science*, Vol. 39, No. 126, 1997, pp. 417–427.

[3] Zhuo, W., and Yiji, Q., "The Design of Waverider Configuration," *Journal of Beijing University of Aeronautics and Astronautics*, Vol. 25, No. 2, 1999, pp. 180–183.

[4] Shi, Y., Miles, J. B., and Isaact, K. M., "Computational Fluid Dynamics Simulation of Turbulent Waverider Flowfield with Sideslip," *Journal of Spacecraft and Rockets*, Vol. 34, No. 1, 1997, pp. 76–82.

[5] Liao, J.-R., Isaact, K. M., Miles, J. B., and Ysai, B.-J., "Navier-Stokes Simulation for Cone-Derived Waverider," *AIAA Journal*, Vol. 30, No. 6, June 1992, pp. 1521–1528.

[6] Rasmussen, M. L., "Waverider Configurations Derived from Inclined Circular and Elliptic Cones," *Journal of Spacecraft and Rockets*, Vol. 17, No. 6, Dec. 1980, pp. 537–545.

[7] Anderson, J. D., Jr., Lewis, M. J., Kothari, A. P., and Corda, S., "Hypersonic Waveriders for Planetary Atmospheres," *Journal of Spacecraft and Rockets*, Vol. 28, No. 4, July–Aug. 1991, pp. 401–410.

[8] Townend, L. H., "The Domain of the Scramjet," *Philosophical Transactions of the Royal Society of London, Series A: Mathematical and Physical Sciences*, Vol. 357, No. 1759, Aug. 1999, pp. 2317–2334.

[9] Harris, R. V., Jr., "On the Threshold-The Outlook for Supersonic and Hypersonic Aircraft," AIAA Paper 89-2071, 1989.

[10] Schindel, L. H., *Tactical Missile Aerodynamics*, edited by M. J. Hemsch and J. N. Nielsen, Vol. 104, Progress in Astronautics and Aeronautics, Chap. Waveriders, AIAA, Washington, D.C., 1986, pp. 198–242.

[11] Cockrell, C. E., Jr., Huebner, L. D., and Finly, D. B., "Aerodynamic Characteristics of Two Waverider-Derived Hypersonic Cruise Configurations," NASA TP 3559, July 1996.

[12] Townend, L. H., "Research and Design for Lifting Reentry," *Progress in Aerospace Sciences*, Vol. 19, 1979, pp. 1–80.

[13] Ramesh, R., Kuhn, M., Abdel-Jawad, M. M., and Morgan, R. G., "Studies on Caret Wings at Superorbital Speeds," AIAA Paper 03-6257, 2003.

[14] Silvester, T. B., and Morgan, R. G., "Computational Hypervelocity Aerodynamics of a Caret Waverider," AIAA Paper 2004-3848, 2004.

[15] Ferguson, F., Chandra, S., Blankson, I., Anderson, J. D., Jr., and Kothari, A. P., "A Design Method for the Construction of Hypersonic Vehicle Configurations," AIAA Paper 95-6009, 1995.

[16] Sager, D. D., "Aerodynamic Investigation of a SSTO Vehicle, Lifting Body Design," AIAA 95-3859, 1995.

[17] Hens, W. D., and Probstein, R. F., *Theory of Hypersonic Flow*, Chinese Science Publishing Company, Beijing, 1979.

[18] Wu, J., *Aerodynamics*, Beijing University of Aeronautics and Astronautics, Beijing, 1992.